# Study of Three-Dimensional Structure in Wire-Array *Z* Pinches by Controlled Seeding of Axial Modulations in Wire Radius

B. Jones,[1,*] C. Deeney,[1] J. L. McKenney,[1] C. J. Garasi,[1] T. A. Mehlhorn,[1] A. C. Robinson,[1] S. E. Wunsch,[1] S. N. Bland,[2] S. V. Lebedev,[2] J. P. Chittenden,[2] S. C. Bott,[2] D. J. Ampleford,[2] J. B. A. Palmer,[2] J. Rapley,[2] G. N. Hall,[2] and B. V. Oliver[3]

[1]*Sandia National Laboratories, Albuquerque, New Mexico 87185, USA*
[2]*Blackett Laboratory, Imperial College, London, SW7 2BZ, United Kingdom*
[3]*Mission Research Corporation, Albuquerque, New Mexico 87110, USA*

(Received 29 October 2004; published 21 November 2005)

Three-dimensional perturbations have been seeded in wire-array $z$ pinches by etching 15 $\mu$m diameter aluminum wires to introduce 20% modulations in radius with a controlled axial wavelength. These perturbations seed additional three-dimensional imploding structures that are studied experimentally and with magnetohydrodynamics calculations, highlighting the role of current path nonuniformity in perturbation-induced magnetic bubble formation.

DOI: 10.1103/PhysRevLett.95.225001 PACS numbers: 52.59.Qy, 52.58.Lq, 52.65.Kj, 52.80.Qj

Wire-array $z$ pinches are the world's most powerful laboratory soft x-ray sources, exemplified by Sandia's *Z* accelerator [1] which is capable of driving 20 MA with a rise time of 100 ns, producing >250 TW and 1.8 MJ of radiation [2]. These high-energy-density plasma sources are used for inertial confinement fusion (ICF) studies, laboratory astrophysics, radiation transport, atomic physics, and other work, while basic research into the fundamental physics that govern their x-ray production is ongoing.

Three-dimensional magneto-hydrodynamic (MHD) evolution of $z$ pinch plasmas and its ultimate impact on x-ray generation has been a topic of increasing recent interest. Experimental observations indicate axial nonuniformity of early-time wire ablation in the form of radial flares of ablating material (0.5 mm axial wavelength in Al wires) streaming from the wires to the array axis [3,4]. This nonuniform ablation leads to the formation of periodic breaks in the wire cores, and subsequent nonlinear magneto-Rayleigh-Taylor-like instability growth in the imploding plasma [5,6]. The radial width of the unstable plasma layer upon reaching the axis at stagnation may play a fundamental role in determining the pulse width and thus peak power of the x-ray radiation generated. Understanding the 3D dynamics of these $z$ pinch plasmas is thus crucial to optimizing their x-ray performance. Computing capability and the sophistication of MHD codes have developed to the level where they are beginning to address many of these physics issues. However, the physical mechanism that seeds the radial flare and implosion instabilities is not well understood, hence *ad hoc* temperature or density perturbations are introduced in order to seed 3D structures which mimic experimental observations.

In this Letter, experimental results from a new technique for studying 3D phenomena in wire-array $z$ pinches through controlled seeding of instabilities are presented along with complementary 3D MHD modeling with the ALEGRA-HEDP [4,7] and GORGON [8,9] codes. Aluminum 5056 wires of 15 $\mu$m diameter have been chemically etched in order to seed 20% perturbations in wire radius with variable axial wavelength. The transition between 15 $\mu$m and 12 $\mu$m diameter sections of wire occurs over $\sim$10 $\mu$m axial length, and the wires are aligned in arrays by using laser diffraction to characterize the diameter along each modulated wire [10]. This process enables the controlled seeding of additional instabilities in a wire-array $z$ pinch by selectively introducing axial mass and current density variation along the wires. Seeding of Rayleigh-Taylor instabilities has previously been performed in planar and convergent laser-driven experiments relevant to ICF capsule implosion, material properties, and laboratory astrophysics [11–13]. In the work presented here, unique 3D experiments have been performed on the 1 MA, 250 ns rise time MAGPIE generator [3,5] that investigate basic wire-array $z$ pinch physics with well-defined initial perturbations in order to facilitate comparison with 3D MHD modeling.

At present, numerical simulation of $z$ pinch implosions is not predictive, as this would require submicron resolution of centimeter-scale wires evolving from solid to plasma while exhibiting 3D MHD instabilities, complex radiation processes, and other physics whose combined treatment is computationally prohibitive. The work presented here represents a step toward enabling validation of future codes, and in the near term offers insight as to the physics underlying the dynamics of implosion instabilities. The perturbations imposed create imploding bubbles that evolve in the same way as instabilities observed in standard wire arrays [e.g., Fig. 5 from [14] ] but whose initial seed is known. The following discussion of experimental data progresses chronologically from the ablation phase to the wire-array implosion. The ALEGRA-HEDP simulation is highly resolved near the wire cores to address dynamics accurately in the early stage, while GORGON is employed to study the final implosion with both imposed and natural modes modeled.

 

The modulations imposed were observed to impact the typical core-corona structure [3,5] of the expanding wire plasma early in time. Figure 1(a) shows an eight-wire Al experiment fielded on MAGPIE, utilizing both modulated and standard extruded wires. The left side of the figure is a sketch of the initial array configuration, which was twisted to allow a better view of individual wires, and the right side is a 532 nm laser shadowgraph recorded 102 ns after the start of the current, or at 54% of the implosion time. This image shows expanded coronal plasma ( $\sim 10^{19}$ cm$^{-3}$ density cutoff) which retains an imprint of the initial wire diameter. The modulated wire on the far right of the image shows smaller diameter coronal plasma corresponding to initially smaller diameter wire. This result was unexpected, as the smaller diameter wire initially carries greater current density than the larger diameter segments, and thus should have more rapid energy deposition so that one might expect faster coronal plasma expansion from the smaller diameter segments.

This wire also illustrates that radial flare formation occurs superimposed on the seeded perturbation, with the 0.5 mm natural wavelength apparently unchanged with varying initial wire diameter. Insensitivity of the radial flare wavelength to initial wire diameter has been previously reported [5], and is seen here for segments of varying diameter carrying constant total current. The seeded wavelength is too long to impact radial flare formation in this case, and the short-wavelength radial flares appear as a decoupled mode. Future experiments with seeded wavelengths shorter than the natural mode will investigate whether the wire ablation can be made more uniform by dominating the natural radial flares, perhaps mitigating implosion instability growth [15]. A coherent mode such as the observed radial flares may promote detrimental instability growth; multimode structures have been suggested to reduce this growth [16] and could be studied experimentally with modulated wires.

A time-resolved self-emission x-ray pinhole image (1.5 $\mu$m Kimfol filter) from the same experiment at 113 ns is shown in Fig. 1(b). Bright emission is seen from the points of discontinuity in wire radius, likely due to enhanced pinching at these points as will be discussed. Elevated temperature corresponding to higher current density in the thinner regions is likely the cause for brighter emission as compared to the adjacent thicker segments.

Wire core breakage at discontinuities in wire radius can be seen in Fig. 1(c), which shows laser shadowgraphy from a correlated 16-wire modulated array at 174 ns (76% of the implosion time). Breaks are also seen in the initially thinner segments of wire. At the time of this image, the fractional mass ablation $\delta m/m$, calculated per a rocket ablation model [5], has reached $\sim$50% in the initially thinner segments of wire, but only $\sim$30% in the thicker segments. This is consistent with observations of standard wire arrays on MAGPIE, in which gap formation is seen at the $\sim$50% mass ablation point, and coincides with the transition from the ablation to the implosion regime.

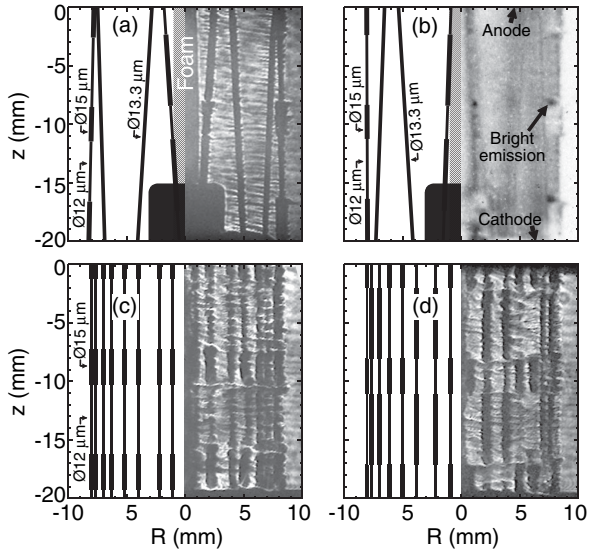


FIG. 1. Sketch of initial wire alignment (left side of each array), and data (right) from several MAGPIE experiments. Wire segments of 12 $\mu$m and 15 $\mu$m diameter were of different axial lengths to aid in their identification in the images. (a) Laser shadowgram at 102 ns showing imprint of wire modulation on coronal plasma. The array was twisted for a better view of individual wires. (b) Soft x-ray pinhole image of the same array at 113 ns; bright emission is seen at discontinuities in wire radius. (c) Laser shadowgram at 174 ns of a correlated array showing breaks at wire radius discontinuities and throughout the thinner wire segments. (d) Laser shadowgram at 173 ns of an anticorrelated array showing transition from ablation to implosion of the thinner wire segments.

Figure 1(d) shows an anticorrelated 16-wire modulated array at 173 ns, in which the initially thinner wire segments are gone, consistent with the onset of implosion of those segments at this time.

Several of the phenomena discussed above can be elucidated by comparison to 3D MHD modeling. We begin with a simplified 3D test problem involving a single modulation period of a MAGPIE eight-wire array using the ALEGRA-HEDP resistive MHD code (fully-Eulerian, Aluminum LMD resistivity, ANEOS 3711 equation of state, Propaceous opacities, single group radiation diffusion). Motivated by 2D $r$-$\theta$ simulations of 12 $\mu$m and 15 $\mu$m wires, the 3D simulation was initiated with 0.43 eV Al wire cores at 7.5% of solid density preexpanded to 100 $\mu$m radius, and 67 $\mu$m radius in the 3.6 mm long central region of the 11.2 mm tall array. The unstructured grid had finest resolution ($\Delta_{x,y} \sim 20$ $\mu$m, $\Delta_z \sim 200$ $\mu$m) within the wire cores. A 125 $\mu$m radius, 10 eV, $2.7 \times 10^{-2}$ kg/m$^3$ coronal plasma sheath surrounded the modulated wire core. As seen in Fig. 2(a), the corona redistributes itself early in time to match the modulation seeded in the current-carrying wire core, as a consequence of the better confining, higher magnetic field surrounding the smaller diameter core segment. This is likely the mechanism responsible for the coronal modulation seen in Fig. 1.

While the evolution discussed thus far appears similar to the behavior of separate arrays of uniform 12 $\mu$m or 15 $\mu$m initial wire diameter, the discontinuities in wire radius cause the appearance of specific 3D structure. As the onset of implosion is approached in Fig. 2(b), breaks are observed to form at the discontinuities, which then evolve into imploding magnetic bubbles in Fig. 2(c). At the implosion time [Fig. 2(d)], the current has been drawn to the axis in the initially thinner wire segments as the magnetic bubbles open insulating gaps in the array, while significant trailing mass is seen in the thicker unimploded wire segments and in the center of the thinner segment. The current has diffused out of this material between the bubbles, following imploding plasma to the axis and leaving a low-density finger in the center of the array. We note that such a current path as shown in Fig. 2(d) (seen also in GORGON simulations) would be highly inductive, and it is unlikely that such a path is realistic in the actual experiment.

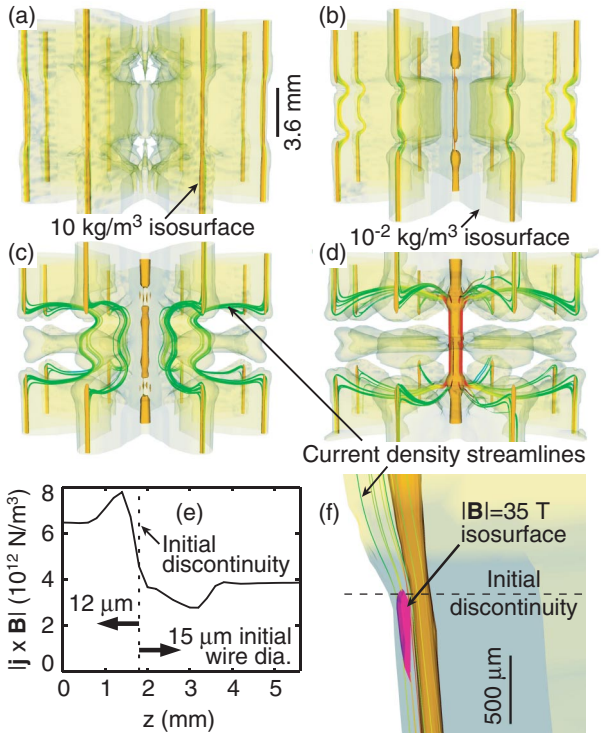


FIG. 2 (color). Evolution of a modulated Al array with an initially thinner central wire segment, as modeled with ALEGRA-HEDP: (a) 185 ns, wire modulation imprints on coronal plasma; (b) 265 ns, breaks form at the discontinuities in wire radius; (c) 280 ns, implosion of magnetic bubbles originating at these discontinuities; and (d) 290 ns, implosion of thinner wire segments drags current to the axis but leaves trailing mass in the center of the segment. (e) Maximum $|\mathbf{j} \times \mathbf{B}|$ along the wire length at 225 ns; Lorentz force enhancement at discontinuities leads to wire core breakage and bubble implosion. (f) Magnetic field enhancement near a wire radius discontinuity, shown at 225 ns, is due to the geometry of the current path in the modulated coronal plasma.

The physical mechanism leading to this 3D behavior is linked to the structure of the current path and magnetic field near discontinuities in wire radius. Figure 2(e) shows the maximum $|\mathbf{j} \times \mathbf{B}|$ versus distance above the array midplane. Stronger Lorentz force at the discontinuities leads to the magnetic bubble formation discussed, and is due primarily to a geometric magnetic field enhancement. Density isosurfaces and current streamlines are shown local to a discontinuity in Fig. 2(f), with a $|\mathbf{B}|$ isosurface (purple) depicting magnetic field enhancement at that point. As material ablates from the wire and is forced toward the array axis by the global magnetic field, a stable current profile develops in which most of the current flows on the side of the wire further from the array axis; current flowing in another location would tend to be swept interior to the array by the Lorentz force. The magnetic field is enhanced at the discontinuity in wire radius, due to summed contributions to the field from differential current elements along the curved current path per the Biot-Savart law. In addition, the axial component of $\mathbf{j} \times \mathbf{B}$ causes flow of some material away from this point early in time, which reduces the diameter of the current-carrying column and also acts to enhance the magnetic field. The stronger $\mathbf{j} \times \mathbf{B}$ force in this region causes enhanced pinching (thus higher temperature and bright x-ray emission) and mass ablation, leading to core breakage and the early onset of imploding bubble formation. A similar magnetic field enhancement mechanism may cause short-wavelength wire core breakage in $m = 0$ necking regions of standard wire arrays [5].

Evidence supporting magnetic bubble formation at discontinuities in wire radius has been observed in a 16-wire modulated Al wire-array experiment on MAGPIE. Time-resolved x-ray pinhole imaging at 214 ns in Fig. 3(a) shows the start of implosion of magnetic bubbles from the discontinuities in the center of the array. By the 241 ns implosion time [Fig. 3(b)], these bubbles have reached the axis, opening large, correlated gaps in the plasma. The finger of trailing mass in the center of the thinner wire segments is seen experimentally, and a large amount of mass is left behind in the initially thicker wire segments. Future measurements of the magnetic field in the gaps will be pursued [17].

The ALEGRA-HEDP simulations discussed above, which exhibit these same phenomena, were conducted using seeded perturbations only, and without any *ad hoc* perturbations to force the growth of 3D structure. This is attractive from a code-validation standpoint, but it is also interesting to investigate the superposition of the seeded mass modulation with a short-wavelength random temperature variation. This has been done for the array of Fig. 3(a) using GORGON, a 3D Eulerian resistive MHD code, configured identically as in [9] with the addition of the mass modulation. The Cartesian grid size is 147 $\mu$m, with a $19 \times 19 \times 13.5$ mm computational volume. The wires are initiated as dense vapor filling columns of single grid cells, with 0.026–0.3 eV random temperature varia-

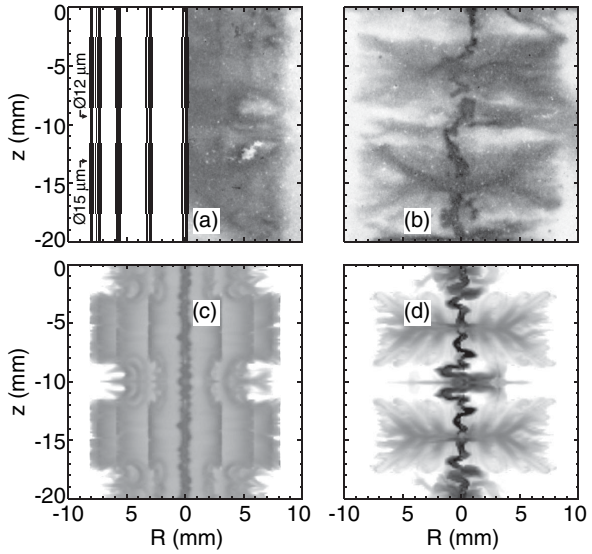


FIG. 3. (a) Initial configuration (left) and x-ray pinhole image (right) at 214 ns of a correlated, modulated 16-wire Al array showing magnetic bubble implosion at discontinuities in wire radius. (b) Self-emission image at the 241 ns implosion time, showing magnetic bubbles compressed to the axis, fingers of mass left in the center of the thinner wire segments, and significant mass left behind from the thicker wire segments. (c),(d) Simulated x-ray self-emission images corresponding to measurements (a),(b), respectively, calculated using the GORGON 3D MHD code.

tions of 880 $\mu$m average wavelength superimposed on the seeded mass modulations. Figures 3(c) and 3(d) display simulated x-ray pinhole images at times corresponding to Figs. 3(a) and 3(b), respectively. In addition to reproducing the 3D structure seeded by the mass modulation, the temperature variation allows additional short-wavelength core breaks to occur [8,9] [Fig. 3(c)], resulting in 3D-unstable partial implosion of the material in the more massive wire sections [Fig. 3(d)] and stimulating $m = 1$ instability growth in the stagnated plasma which in simulations ultimately limits the compression.

Modification of the x-ray pulse shape by introduction of axial mass modulations into these wire-array $z$ pinches was observed using a 6 $\mu$m Kimfol-filtered photoconducting detector (PCD). The 16-wire arrays discussed above were compared to a 16-wire, 16 mm nominal diameter array of standard 13.3 $\mu$m diameter Al 5056 wire (approximately the same total mass as the modulated arrays). Though the correlated arrays appeared to have slightly faster rise time, all of the modulated arrays produced $\sim$35% lower peak power than the standard array. This result is in contrast to the GORGON simulations, which predicted higher x-ray power due to the effect of the magnetic bubbles forcing the current into a narrow column on axis. This discrepancy may be related to the observed tendency of the code to leave too little trailing mass in the gaps opened by the bubbles leading to artificially high current compression, or may be an indication that the experiment did not possess adequate symmetry to retain this insulating gap and force a high current density on axis. Comparison with simulation is ongoing, and higher wire number, more symmetric experiments will be fielded on a higher current generator.

Modulated wires provide a unique format for experimentally and numerically studying 3D effects in wire-array $z$ pinches. In the work presented here, MHD modeling has provided plausible physical insight into 3D dynamics induced by controlled perturbations. The role of nonuniformity in the current path has been linked to coronal plasma modulation [3], wire core breakage [3], and magnetic bubble formation [14], phenomena which impact standard wire-array $z$ pinches and could influence energy deposition in the plasma [18]. It is possible that nonuniform current density due to wire grain structure, impurity inclusions [10], resistivity, or density perturbations similarly seeds the radial flare and implosion instabilities in standard wire arrays. Future work will further investigate radial flare formation through the seeding of short-wavelength perturbations, the physics of magnetic bubble formation, x-ray pulse shape modification, and other novel 3D wire-array $z$ pinch geometries.

The authors would like to thank the Materials Processing and Coatings Laboratory team, Ktech Corp., Albuquerque, NM, for manufacturing wires for this work, along with A. L. Velikovich and S. A. Slutz for valuable discussion. Sandia is a multiprogram laboratory operated by Sandia Corporation, a Lockheed Martin Company, for the US DOE's National Nuclear Security Administration under Contract No. DE-AC04-94AL85000. Work at Imperial College is partially supported by the US DOE through cooperative agreement DE-FC03-02NA00057.

*Electronic address: bmjones@sandia.gov

[1] R. B. Spielman *et al.*, Phys. Plasmas **5**, 2105 (1998).
[2] C. Deeney *et al.*, Phys. Rev. Lett. **81**, 4883 (1998).
[3] S. V. Lebedev *et al.*, Phys. Rev. Lett. **85**, 98 (2000).
[4] C. J. Garasi *et al.*, Phys. Plasmas **11**, 2729 (2004).
[5] S. V. Lebedev *et al.*, Phys. Plasmas **8**, 3734 (2001).
[6] D. B. Sinars *et al.*, Phys. Rev. Lett. **93**, 145002 (2004).
[7] A. C. Robinson and C. J. Garasi, Comput. Phys. Commun. **164**, 408 (2004).
[8] J. P. Chittenden *et al.*, Phys. Plasmas **8**, 2305 (2001).
[9] J. P. Chittenden *et al.*, Plasma Phys. Controlled Fusion **46**, B457 (2004).
[10] B. Jones *et al.*, Rev. Sci. Instrum. **75**, 5030 (2004).
[11] C. Cherfils *et al.*, Phys. Rev. Lett. **83**, 5507 (1999).
[12] D. H. Kalantar *et al.*, Phys. Plasmas **7**, 1999 (2000).
[13] H. F. Robey *et al.*, Phys. Plasmas **8**, 2446 (2001).
[14] S. V. Lebedev *et al.*, Plasma Phys. Controlled Fusion **47**, A91 (2005).
[15] D. Ryutov and A. Toor, Phys. Plasmas **5**, 22 (1998).
[16] M. R. Douglas, C. Deeney, and N. F. Roderick, Phys. Plasmas **5**, 4183 (1998).
[17] A. Y. Labetsky *et al.*, IEEE Trans. Plasma Sci. **30**, 524 (2002).
[18] L. I. Rudakov *et al.*, Phys. Rev. Lett. **84**, 3326 (2000).